

Journal of Materials Chemistry A

Accepted Manuscript



This is an *Accepted Manuscript*, which has been through the Royal Society of Chemistry peer review process and has been accepted for publication.

Accepted Manuscripts are published online shortly after acceptance, before technical editing, formatting and proof reading. Using this free service, authors can make their results available to the community, in citable form, before we publish the edited article. We will replace this *Accepted Manuscript* with the edited and formatted *Advance Article* as soon as it is available.

You can find more information about *Accepted Manuscripts* in the [Information for Authors](#).

Please note that technical editing may introduce minor changes to the text and/or graphics, which may alter content. The journal's standard [Terms & Conditions](#) and the [Ethical guidelines](#) still apply. In no event shall the Royal Society of Chemistry be held responsible for any errors or omissions in this *Accepted Manuscript* or any consequences arising from the use of any information it contains.

ARTICLE

Open-circuit voltage shifted by the bending effect for flexible organic solar cells

Cite this: DOI: 10.1039/x0xx00000x

Wei-Yang Chou^{a,*}, Chia-Te Yen^a, Fu-Chiao Wu^a, Horng-Long Cheng^b, Shyh-Jiun Liu,^c and Fu-Ching Tang^b

Received 00th January 2012,

Accepted 00th January 2012

DOI: 10.1039/x0xx00000x

www.rsc.org/

The shift of the open-circuit voltage (V_{oc}) of flexible organic solar cells (OSCs) under bending conditions was investigated by fabricating bi-layer heterojunction and polymer-based OSCs on flexible polyethylene terephthalate (PET) substrates. To realize the performance variations of flexible solar cells characterized by important parameters, V_{oc} was measured when the substrate was bent under various curvatures. The V_{oc} was increased and decreased by using tensile and compressive stresses, respectively. The ratio of increase for V_{oc} is larger than the ratio of reduction, thus indicating that the intermolecular distance of an organic semiconductor is difficult to change because of the strong electrostatic repulsive force. A quantitative analysis of energy level by photoluminescence spectrum, UV-visible absorption spectrum, and quantum chemical calculation at various bending states was used to explain the V_{oc} as a function of bending curvature. The peak shifts of UV-visible absorption and photoluminescence spectra provide direct evidence on the variation in energy levels when devices are bent, which causes V_{oc} shifts. For bended organic semiconductor films, the bending curvature-dependent intermolecular distance was studied by Raman spectroscopy by analyzing the intermolecular couple energy. This study shows that the change of V_{oc} cannot be neglected in the application of flexible OSCs on a flexible loading circuit.

Introduction

Organic solar cell (OSC) devices have been rapidly developed in the past few years. Both small molecule and polymer organic materials have significant potential in photovoltaic cell fabrication because of their broad absorption band, which coincides with the solar spectrum¹⁻⁴, and simple fabrication technologies, such as spin-coating, inject printing, thermal evaporation, or roll-to-roll process^{5,6}. Furthermore, the power conversion efficiency (PCE) of OSC devices has been rapidly improving⁷⁻⁹. The plasticity and low fabrication cost of OSCs are the main factors that give these materials significant potential in next-generation solar power. The innately bendy characteristics of organic materials benefit OSCs that are applied on flexible electronics^{10, 11}, such as OSC formations on polyethylene terephthalate (PET) substrates, which can bend and stretch without breaking^{12, 13}. Flexible solar cells have been developed to power satellites. Flexible solar cells are lightweight, can be rolled for launch, and are easily deployable. Thus, flexible solar cells are suitable for various applications. Moreover, flexible solar cells can also be sewn into backpacks or outerwear. Flexible devices offer advantages to the development of portable merchandise. Flexible electronic devices frequently encounter bending. Thus, the influence of bending on the electronic functionality of flexible devices is an important issue. Previous studies have shown that the most obvious bending effect on OSC devices is the change of short-circuit current density (J_{sc})¹⁴. The J_{sc} of a flexible device will change when the device is distorted by an external bending force. However, few reports have focused on the variation of open-circuit voltage (V_{oc}).

The physical mechanism of V_{oc} when a flexible device is under bending states is also unclear.

When a flexible device is bent, the microstructure of its organic films will be altered. Microstructure properties influence charge dissociation, charge transport, charge collection, and device performance¹⁵⁻¹⁷. Obvious changes can be observed in many physical and electronic features while a flexible device is bent, for example, changes in J_{sc} and V_{oc} . This study investigated the physical mechanisms of V_{oc} variation under bending. The results of this study will elucidate the issue of the bending effect on flexible OSC devices. Moreover, V_{oc} is an important parameter for loading devices on a flexible circuit because the loading process is a decisive factor in the performance of loading devices.

Pentacene and N,N'-diheptyl-3,4,9,10-perylenetetracarboxylic diimide (PTCDI-C₇H₁₅) were used as the donor and acceptor of active layer materials, respectively, for flexible OSCs fabricated on flexible PET substrates. Apparent shifts in V_{oc} (*i.e.* ΔV_{oc}) were obtained for flexible OSCs bent under tensile and compressive stresses. The V_{oc} of OSCs increased and decreased when the device was under tensile bending and compressive bending, respectively. To illustrate the mechanism of ΔV_{oc} under a bending state and identify the variations in the energy gap, photoluminescence (PL) and UV-visible absorption spectra were used to analyze the optical property variations of organic thin films during bending. During bending, the microstructure variation of the active layer was investigated by using Raman spectroscopy. The results of Raman

and optical measurements support the effect of microstructure changes on V_{oc} during bending states. Quantum mechanical calculations were used to verify the relationship between the change in molecular structure and the variation of V_{oc} . The analysis results for the effect of the bending effect on flexible OSCs can be potentially applied to photovoltaic devices that are used under winding to determine real power output.

Experimental methods

2.1 Devices Fabrication

A flexible PET film that was previously coated with an Al-doped ZnO (AZO) layer with a sheet resistance of $25 \Omega/\square$ was used as the OSC substrate. The AZO layer served as the anode of OSCs and was patterned by using hydrochloric etching. The patterned substrates were cleaned in an ultrasonic bath with de-ionized water, acetone, and isopropanol for 15 min each. The substrates were then dried inside an oven at 80°C . After drying, the substrates were treated by oxygen plasma for 5 min. Poly (3,4-ethylenedioxythiophene) (PEDOT:PSS, H.C. Starck) was spin-coated on PET substrates at 500 rpm/5 s and then spun at 2500 rpm/60 s to form a 30 nm-thick film. All samples were baked at 150°C for 30 min to remove residual solvent from the film. A 45 nm-thick pentacene layer, a 45 nm-thick PTCDI- C_7H_{15} layer, and an 8 nm BCP layer were deposited in sequence at a deposit rate of $0.5 \text{ \AA}/\text{s}$ under a pressure of 5×10^{-6} Torr. The top electrode was constructed by using 10 nm-thick Ag and 60 nm-thick Al films. The top electrode was used as a cathode and was thermally deposited through a shadow mask to define the active area. The sizes of the active area

of the small molecule-based OSCs are $0.5 \text{ mm} \times 0.5 \text{ mm}$. To extend our results, polymer-based OSCs consisted of poly(3-hexylthiophene) (P3HT) blends with indene- C_{60} bis-adduct as active materials were fabricated on the same flexible substrate. The sizes of the active area of the polymer-based OSCs are $3 \text{ mm} \times 2 \text{ mm}$.

2.2 Measurements and Analysis

Several acrylic holders with different curvatures were used in all electrical and optical measurements to bend the device into specific tensile or compressive conditions. Holder curvatures K of 0, 0.33, 0.5, and 1 cm^{-1} were used in this study. Holder curvatures were defined as the reciprocal of the curvature radius. The symbols “+” and “-” marked in front of the curvature represent that the device was bent under tensile and compressive states, respectively (Figure 1). The current density–voltage (J – V) characteristics of the devices were measured in a nitrogen-filled dark glove box. The J – V curves were obtained by using a Keithely 2400 source meter, which were controlled via Labview. An Oriel solar simulator was used to illuminate the devices from the AZO side with a light intensity of $100 \text{ mW}/\text{cm}^2$ in AM 1.5 G condition. To realize the bending effect on OSCs, PL and Raman measurements (Jobin Yvon LabRAM HR system) were performed on active OSC layers to obtain the optical responses under bending states. The organic films were excited by 532 and 632.8 nm lasers for PL and Raman, respectively. The spectrometer resolution of this measuring system was 0.2 cm^{-1} . The UV-visible absorption spectra were measured by using a Cintra

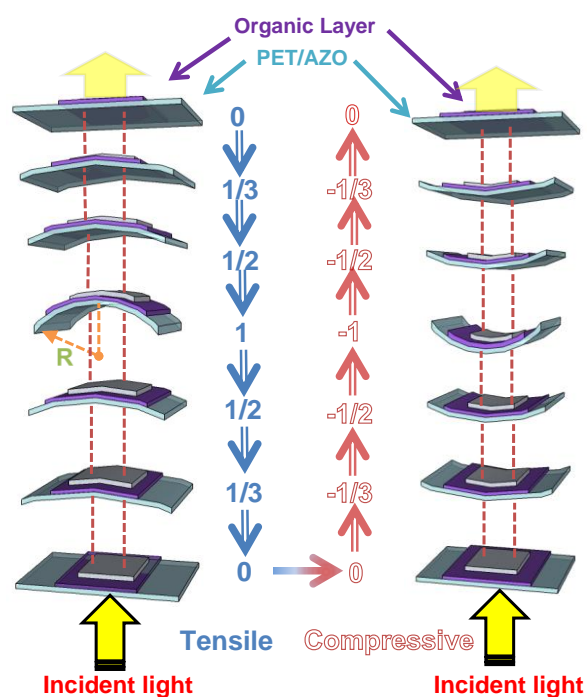


Fig. 1. Schematic illustration of a flexible organic solar cell which is bent under various curvature states. The curvature K of the solar cell is defined as the reciprocal of radius R of the curvature.

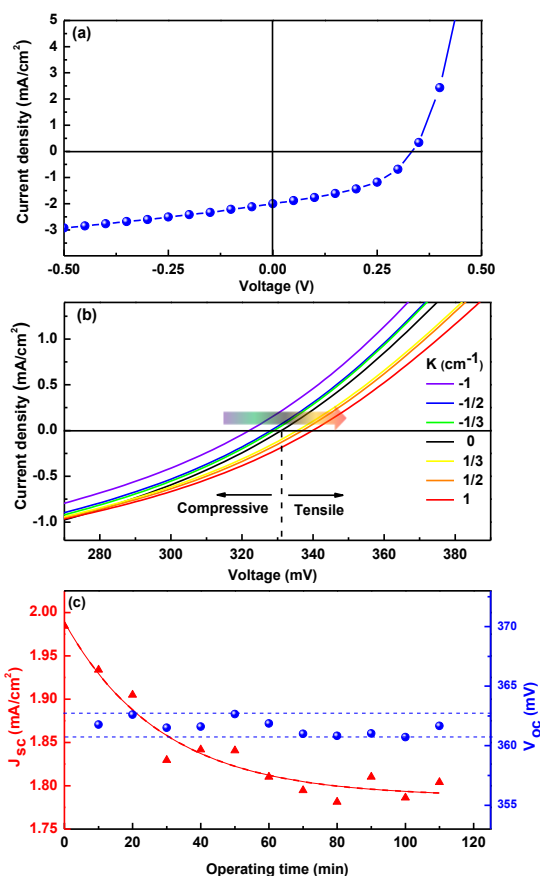


Fig. 2. (a) Current density–voltage characteristic of a small molecule photovoltaic cell at the flat state. (b) Curvature dependence of open-circuit voltage (V_{oc}) for the flexible solar device. (c) The changing of J_{sc} and V_{oc} of unbent device which was under long time operating.

202 spectrometer with a resolution of 1 nm to determine the absorption spectrum variation at the bending state.

2.3 Theoretical Calculation

The neutral geometries of a single pentacene molecule and a single PTCDI molecule were individually optimized by using density functional theory (DFT) at the B3LYP/6-31G(d) level. Thereafter, two pentacene molecules constructed as a pentacene dimer and two PTCDI molecules as a PTCDI dimer were placed together to construct a two-dimer system. The intermolecular spacing of the two dimers was set to identical, and the spacing between the two dimers was 2 Å. The highest occupied molecular orbital (HOMO) and the lowest unoccupied molecular orbital (LUMO) of pentacene and PTCDI in the two-dimer system were calculated by DFT at the CAM-B3LYP/6-31G(d) level by using the counterpoise method and considered the dimer-centered basis set. The difference between the HOMO and LUMO of a molecule was defined as the band gap, and the difference between the HOMO of pentacene and the LUMO of PTCDI was denoted as the built-in energy (V_{bi}). All computations were performed by using the program suite of Gaussian 09.¹⁸

Results and discussion

The J_{sc} , V_{oc} , fill factor (FF), and PCE of an unbent OSC are 2 mA/cm², 333 mV, 0.44, and 0.294%, respectively [Figure 2(a)]. The J - V characteristics of devices bent under different curvatures are shown in Figure 2(b). The V_{oc} value shifts in different trends when the OSC device underwent tensile or compressive bending. In organic OSCs, the change of V_{oc} is hardly obtained because the S value [in Eq. (1)] for organic heterojunctions is small; approximately 0.1¹⁹.

$$V_{oc} = S_0 \times V_{oc1} - S_1 \times V_{b1} - S_2 \times V_{b2} + C \quad (1)$$

where C is a constant that describes the interface potential of the ideal ohmic contact, and the parameters S_0 , S_1 , and S_2 are the base on the index of the interface behavior.²⁰ The V_{oc1} , V_{b1} , and V_{b2} in Equation 1 are the potential difference between acceptor LUMO and donor HOMO, the work function differences of donor/anode and acceptor/cathode, respectively. The V_{oc} value decreases from 335 mV to 324 mV (a decrease of 2.9%) when the devices were bent from a flat state to a compressive state. Contrary to the compressive condition, the V_{oc} increases by 3.42% when the flexible OSC was

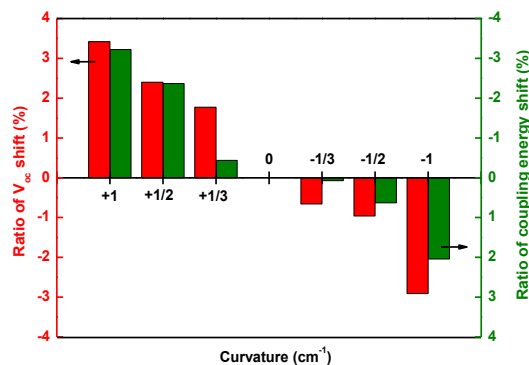


Fig. 3. The chart shows the curvature dependences of ratio of V_{oc} shift (left axis) and ratio of coupling energy shift (right axis) for a flexible organic solar cell.

significantly bent to a tensile state with curvature of +1 cm⁻¹ (Figure 3). When the bending force applied on the OSC was released, the electrical characteristic returned to its original state, thus indicating that the band structure of an organic semiconductor could be affected by the bending effect. To investigate the effect of incident light intensity in the V_{oc} of bent devices, Figure 2(c) shows that although the decay of J_{sc} is observed under a long time interval, V_{oc} remains constant. Therefore, no apparent correlation between J_{sc} and V_{oc} was observed in our flexible OSC. The active areas of small molecule- and polymer-based OSCs are 0.25 mm² and 6 mm², respectively, which result in corresponding light incident angles of approximately 1.5° and 8.5°, respectively, at a bending curvature of 1 cm⁻¹. We believe that the J_{sc} will be slightly affected by the effect of incident light intensity because of a small variation in the light incident angle. Despite this effect, the change in V_{oc} remains hardly observable; accordingly, the effect of incident light intensity on the V_{oc} shift at bending states can be ignored.

To realize the behavior of the V_{oc} shift induced by the bending effect, the PL and UV-visible absorption spectroscopy measurements were performed on organic semiconductor films to study the fine structural changes under bending states. Figure 4a shows the PL spectra of a PTCDI-C₇H₁₅/pentacene semiconductor thin film that was bent to various curvatures. Given that the luminescent signal of the PTCDI-C₇H₁₅ film was stronger than the luminescent signal of the pentacene film, the PL signals are dominated by PTCDI-C₇H₁₅. The main PL peaks of PTCDI-C₇H₁₅ film are located between 670 and 700 nm. Significant shifts of the peaks are observed within the PL spectra when various bending curvatures are conducted on the organic semiconductor film. A conspicuous blueshift of the PTCDI-C₇H₁₅ peaks appears on the PL spectra at the tensile region. An opposite redshift phenomenon is observed in the compressive region, thus indicating that the band gap of PTCDI-C₇H₁₅ increases in tensile bending and decreases in compressive bending. The gray curvy line in Figure 4a shows the level of the peak shift at different bending states. Figure 4b shows the UV-visible absorption spectra of the PTCDI-C₇H₁₅/pentacene film at various bending states. The

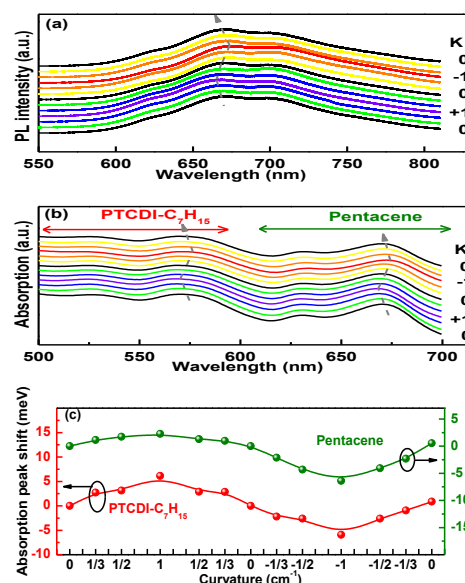


Fig. 4. (a) Photoluminescence spectra (excited by laser wavelength of 532 nm) and (b) light absorption spectra of a pentacene/PTCDI-C₇H₁₅ film formed on a flexible PET substrate. (c) Curvature dependence of main absorption peak shifts for pentacene (right axis) and PTCDI-C₇H₁₅ (left axis) films. All measurements are obtained under various compressive and tensile curvatures.

absorption bands of the PTCDI-C₇H₁₅ and pentacene films range from 500 nm to 600 nm and 600 nm to 700 nm, respectively^{4,21}. The peak shift trend of the UV-visible spectra varies with the bending curvature and is the same as that of the PL spectra. Furthermore, the absorption peak shift of pentacene follows that of PTCDI-C₇H₁₅ (Figure 4c). Both optical results indicate that the band gaps of donor and acceptor materials were reduced when the device was compressed. The band gap of both active layers increased during the tensile condition compared with the compressive condition. To clarify the mechanism of V_{oc} shift affected by the bending effect, the V_{oc} shift of the bent device and the peak shift of PL are compared in Figure 5. Interestingly, the variation of V_{oc} as a function of bending curvature closely approaches the behavior of the PL peak shift for the PTCDI film. This result indicates that the decrease in V_{oc} is caused by the reduction of the band gap for both active films during compressive states. When both active films are bent at tensile state, the enlargement of the band gap increases V_{oc} . Thus, the V_{oc} shift of OSC can be attributed to the band gap variations of the active layers at the bending state. Previous researches have reported that band gaps are strongly dependent on the molecular distance of organic semiconductors²². Moreover, the molecular distance within a thin film may be changed by external compressive or tensile stress. Therefore, further studies of the relationship between the changes of band gaps and molecular distance is needed to clarify the mechanism of V_{oc} shift at bending states.

To investigate the relationship between molecular distance changes and band gap shifts within a bending device, Raman spectroscopy was used to analyze the bending effect of organic semiconductor films. Figure 6 shows the normalized Raman spectra of pentacene with the vibrational band ranging from 1140 cm⁻¹ to 1190 cm⁻¹ is dedicated by the C–H in-plane bending of pentacene²³. Both the 1158 and 1178 cm⁻¹ bands are H-atoms with fully symmetric vibrations located at the end and on both sides of the pentacene, respectively. The vibrational band at 1155 cm⁻¹ (denoted as ν_1 band) is split from the 1158 cm⁻¹ band, which originates from the different interaction energy between the two adjacent pentacene molecules in a unit cell and is analogous to Davydov splitting. Thus, the ν_1 band appears in all spectra when the pentacene molecules are stacked to form a thin film. Given that the pentacene film is subjected to the compressive force, the ν_1 band has an obvious redshift away from the 1158 cm⁻¹ band (Figure 6a). By contrast, the ν_1 band has a blueshift close to the 1158 cm⁻¹ band when the pentacene film is bent at the tensile state (Figure 6b). The

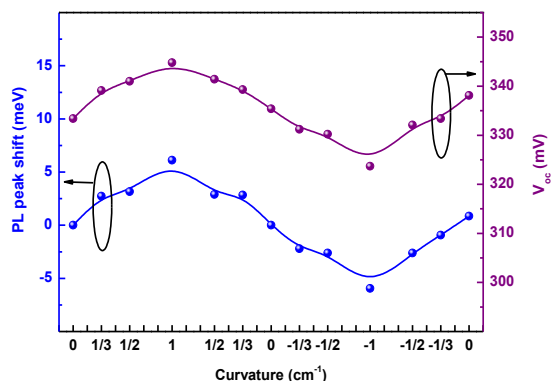


Fig. 5. Compared with the curvature dependence of V_{oc} shift (right axis) for a OSC, the same trend is observed for curvature dependence of PL peak shift for the PTCDI-C₇H₁₅ film. The figure shows curvature dependence of V_{oc} and PL main peak shift for the OSC, respectively.

1158 cm⁻¹ is the vibration signal of a single pentacene molecular; therefore, no apparent shift can be observed in this vibrational band under bending states. According to the concept of Davydov splitting, the coupling energy (ω_1) of pentacene molecules can be calculated from the splitting level of the ν_1 and 1158 cm⁻¹ bands, thus indicating that the coupling energy increases when the device is under compressive bending. In weak coupling, the vibrational coupling energy ω_1 can be calculated by the following equation:

$$\Delta\omega \approx \frac{\omega_1^2}{2\omega_0} \quad (2)$$

where $\Delta\omega$ and ω_0 are the amount of Davydov splitting and internal molecular band frequency ($\omega_0 = 1158$ cm⁻¹ in this case), respectively. The ω_1 value of unbent pentacene is 11.38 meV. Compared with the ω_1 value of unbent pentacene, ω_1 increases 0.23 meV, (an increase of 2.04%) at a compressive bending of curvature -1 and decreases 0.37 meV (a decrease of 3.22%) at a tensile bending of curvature $+1$ (Figure 3), thus indicating that the intermolecular distance of pentacene is reduced by compressive bending to result in the increase of coupling energy. The variation of coupling energy and V_{oc} shift has the same variation behavior as the bending curvature. It is noted that the vibrational band and V_{oc} shifts at tensile bending are more obvious than those at compressive bending because of the difficulty in changing the distance of pentacene molecules in a unit

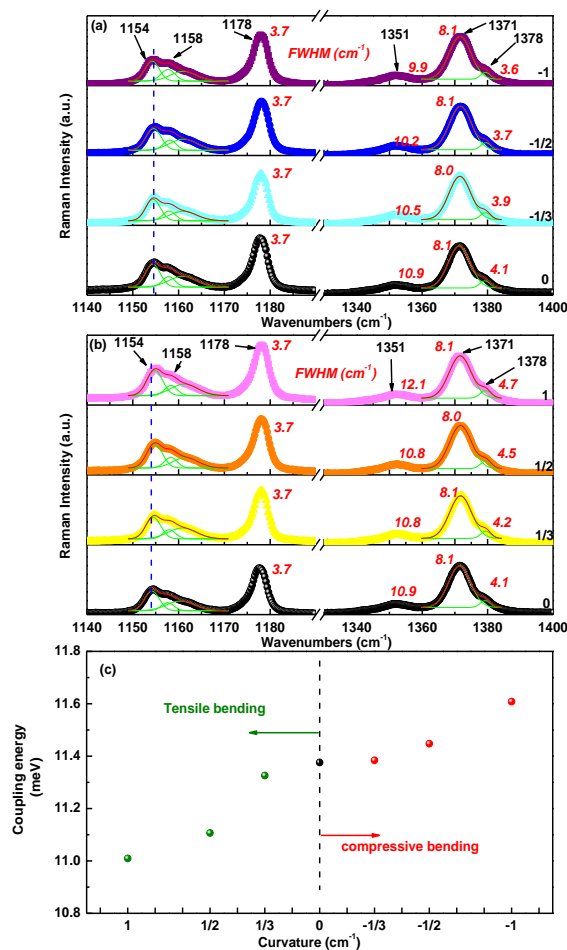


Fig. 6. The Raman spectra of a pentacene film measured under (a) compressive state and (b) tensile state. The Gaussian/Lorentzian function was used to fit the atomic vibration modes (green lines). (c) Curvature dependence of the coupling energy of pentacene molecules.

cell. This difficulty is caused by the strong electrostatic repulsive force between pentacene molecules that are subjected to compressive force. Thus, the molecular spacing can be easily changed by tensile force compared with compressive force. Furthermore, the intensity of the 1178 cm^{-1} band increases and decreases with the increasing curvatures of tensile bending and compressive bending (raw data not shown), respectively. This result indicates that the vibrational freedom degree of the H-atoms at both sides of the pentacene increases with the increasing molecular spacing in tensile bending. Thus, molecular spacing is affected by substrate bending, which leads to changes in electronic coupling energy and band gap.

The C–C aromatic stretching modes of pentacene are located between 1330 and 1390 cm^{-1} (Figure 6). Three main vibrational bands at 1351 , 1371 , and 1379 cm^{-1} can be easily observed in a Raman spectrum. Among these bands, 1351 and 1378 cm^{-1} bands are affected by horizontal stress forces easily, 1351 cm^{-1} band especially. The full width at half maximum (FWHM) of 1351 and 1378 cm^{-1} bands increases with increasing tensile bending curvature. Nevertheless, FWHM decreases with increasing compressive bending curvature. This result shows that the degree of C–C vibration freedom increases when the pentacene film is under a tensile bending state, thus indicating that the intermolecular spacing of pentacene in a unit cell increases at tensile bending conditions again. Both Raman shifts of C–H and C–C aromatic stretching modes imply that the molecular spacing and energy level of pentacene film changes by applying compressive or tensile stress. In conclusion, for the variations of Raman bands, PL, and absorption characteristic peaks at bending conditions, the band gap and V_{oc} decrease with decreasing molecular distance under compressive bending. By contrast, the molecular distance was enlarged under the tensile bending to increase the band gap and V_{oc} . In OSC devices, the difference between the HOMO of the donor and the LUMO of the acceptor is considered a built-in potential, which is an important

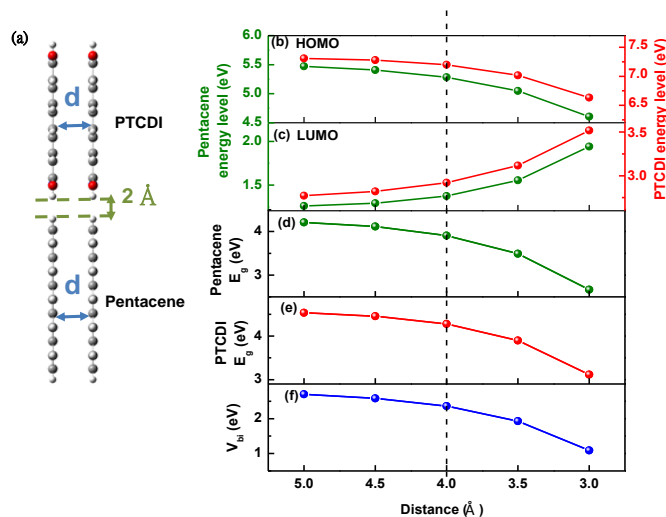


Fig. 7. (a) The schematic diagram of quantum mechanical calculations model. The changing of (b) HOMO energy level, (c) LUMO energy level, (d) pentacene energy band gap (E_g), (e) PTCDI E_g and (f) the built-in potential (V_{bi}) varied with the molecular distance.

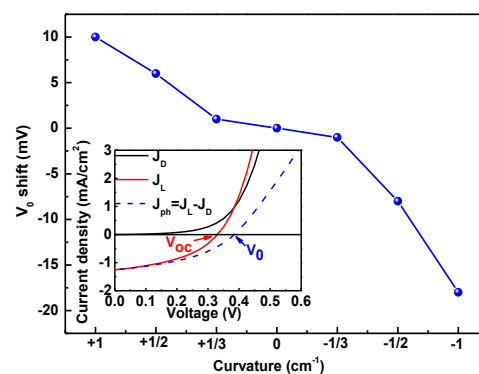


Fig. 8. Curvature dependence of the compensation voltage (V_0). The inset shows the J - V curve of the unbent OCS of unilluminated (J_D), illuminated (J_L), and offset ($J_{ph} = J_L - J_D$), where the arrows indicate the V_{oc} and V_0 .

parameter of OSC^{24, 25}. Earlier studies indicate that the V_{oc} of OSC devices is generally influenced by the built-in potential²⁶. However, how the bending curvature affects the HOMO and LUMO of active layers is still unclear.

To realize the changes of the HOMO and LUMO of PTCDI- C_7H_{15} /pentacene films at various bending conditions, a simple face-to-face structure for a dimer in a unit cell was used to calculate the HOMO and LUMO at a bending state (Figure 7a). The set distance of the dimers at a flat state is 4 \AA , and the two dimers are vertically separated by a gap of 2 \AA . The quantum mechanical calculations display that the HOMO of the pentacene and PTCDI- C_7H_{15} dimers increases with increasing dimer distance and that LUMO decreases with increasing dimer distance (Figures 7b and 7c, respectively). Figures 7d and 7e show the band gaps of the pentacene and PTCDI- C_7H_{15} dimers as a function of the dimer distance, respectively. The dimer distance is obtained from the difference between HOMO and LUMO. The band gaps of pentacene and PTCDI- C_7H_{15} increase with increasing dimer distance, thus indicating that the band gap decreases in the compressive stress performed on organic films and increases in the tensile case. These simulation results of the band gap completely coincide with the results obtained from PL and the absorption measurements in banding states. Figure 7f shows V_{bi} as a function of the dimer distance that is defined as the difference between the HOMO of donor and the LUMO of acceptor. The V_{bi} also increases with increasing dimer distance; this result corresponds with the result of the V_{oc} shift at bending states because V_{oc} is proportional to V_{bi} . When the current-voltage curves in the dark intersect with the curves under illumination, the compensation voltage V_0 is obtained in the inset of Figure 8^{27, 28}. A comparison between the curvature-dependent V_0 (Figure 8) and the curvature-dependent V_{oc} (Figure 3) shows that both voltage trends tend toward coincidence. Moreover, the value of V_0 is very close to the built-in potential V_{bi} ²⁸. The trends of the curvature-dependent V_0 and V_{bi} are almost the same; that is, the simulated HOMO and LUMO levels for the donor and acceptor under bending states are reasonable.

We extended this investigation and showed that the V_{oc} of polymer-based flexible OSCs can also be shifted by the bending effect. Polymer-based OSC consists of poly(3-hexylthiophene) (P3HT) blends with indene- C_{60} bis-adduct, which was formed on the same flexible polyethylene terephthalate substrate. The polymer-based OSC had a power conversion efficiency of 1.82% ,

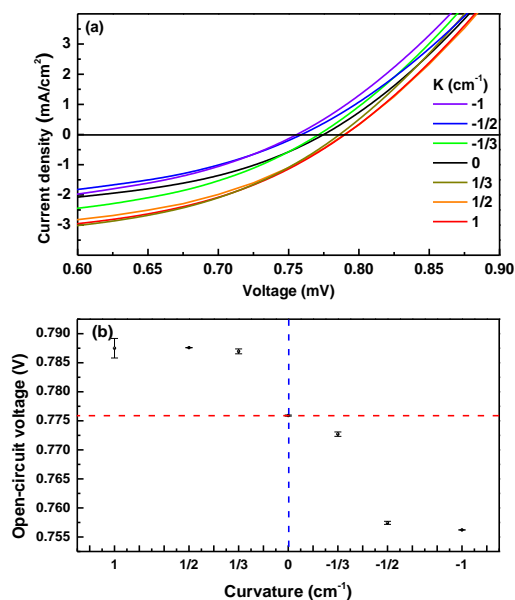


Fig. 9. (a) Current density—voltage characteristic of bending polymer-based photovoltaic cell under different curvatures. (b) Curvature dependence of V_{oc} for the flexible polymer-based solar device.

J_{sc} of 5.0 mA/cm^2 , and an FF of 46.2%, which are smaller than that fabricated on a glass substrate with indium tin oxide (ITO) electrode²⁹. Figure 9a shows the influence of bending effect on the J - V curve of polymer-based flexible OSC. Figure 9b shows that the behavior of V_{oc} shift under bending state is similar to that of a small molecule-based OSC, i.e., the increase and decrease of V_{oc} at tensile and compressive states, respectively. Saturation phenomenon was observed for the V_{oc} at both bending states when the bending curvature was higher than 0.5 cm^{-1} . Hence, the V_{oc} shift effect induced by bending can be used to analyze bilayer heterojunction OSCs and polymer-based devices.

Conclusions

In summary, we performed a series of V_{oc} measurements at different bending curvatures that play important roles in the performance of flexible OSCs at bending states. By increasing the bending curvature of the PET substrate, V_{oc} is enhanced at tensile bending and is reduced at compressive bending. The asymmetry of the variation ratio for V_{oc} at tensile and compressive states indicates that the intermolecular distance is difficult to change at compressive conditions because of the strong electrostatic repulsive force between semiconductor molecules, such as pentacene molecules and PTCDI- C_7H_{15} molecules. PL spectroscopy, absorption spectroscopy, and Raman spectroscopy were used to investigate the intermolecular distance of organic semiconductor films at bending states. The intermolecular distance increases in the tensile condition and decreases in the compressive case, thus resulting in corresponding variations in the band gap and V_{oc} . We also predicted the HOMO and LUMO eigenvalues of pentacene and PTCDI- C_7H_{15} dimers by employing DFT function at various bending conditions to simulate the variations of band gap and V_{bi} . The HOMO level increases with increasing intermolecular distance. On the contrary, the LUMO level decreases with increasing intermolecular distance. According to the proportion of V_{oc} to V_{bi} , the swing of V_{oc} at the bending states can be explained by quantum mechanical calculations. Thus, these experimental and quantum mechanical calculation methods can be

powerful tools for analyzing molecular electronics and predicting molecular-orbital eigenvalues, respectively, for flexible devices at bending states.

Acknowledgements

The authors acknowledge financial support from the National Science Council, Taiwan, through Grant NSC 102-2112-M-006 - 002-MY3. The assistance of the Center for Micro/Nano Technology Research, National Cheng Kung University, for support through equipment and cooperation is gratefully acknowledged.

Notes and references

^a Department of Photonics, Advanced Optoelectronic Technology Center, National Cheng Kung University, Tainan 701, Taiwan. E-mail: weiyang@mail.ncku.edu.tw; Fax: +886 6 2095040; Tel: +886 6 2757575 ext.63912

^b Department of Physics, National Cheng Kung University, Tainan 701, Taiwan.

^c Department of Greenery, National University of Tainan, Tainan 700, Taiwan.

- S. Karak, V. S. Reddy, S. K. Ray and A. Dhar, *Org. Electron.*, 2009, **10**, 1006.
- S. Yoo, B. Domercq and B. Kippelen, *Appl. Phys. Lett.*, 2004, **85**, 5427.
- P. Peumans, A. Yakimov and S. R. Forrest, *J. Appl. Phys.*, 2003, **93**, 3693.
- A. K. Pandey, S. Dabos-Seignon and J.-M. Nunzi, *Appl. Phys. Lett.*, 2006, **89**, 113506.
- D. Angmo, S. A. Gevorgyan, T. T. Larsen-Olsen, R. R. Sondergaard, M. Hosel, M. Jorgensen, R. Gupta, G. U. Kulkarni and F. C. Krebs, *Org. Electron.*, 2013, **14**, 984.
- B. Yoon, D. Y. Ham, O. Yarimaga, H. An, C. W. Lee and J. M. Kim, *Adv. Mater.*, 2011, **23**, 5492.
- B. Gholamkhash and P. Servati, *Org. Electron.*, 2013, **14**, 2278.
- S. P. Yang, Y. Zhang, T. Jiang, X. F. Sun, C. Q. Lu, G. Li, X. W. Li and G. S. Fu, *Chinese Sci. Bull.*, 2014, **59**, 297.
- Z. C. He, C. M. Zhong, S. J. Su, M. Xu, H. B. Wu and Y. Cao, *Nat. Photonics*, 2012, **6**, 591.
- S. F. Chen, X. Guo, Q. Wu, X. F. Zhao, M. Shao and W. Huang, *Chinese Phys. B*, 2013, **22**, 128560.
- A. Chida, T. Aoyama, S. Eguchi, T. Inoue, N. Senda, T. Sakuishi, H. Ikeda, S. Shitagaki, N. Ohsawa, H. Inoue, K. Suzuki, H. Seo, T. Sasaki, Y. Nonaka, H. Nakashima, T. Suzuki, T. Watabe, S. Seo, Y. Hirakata, S. Yamazaki, S. Yasumoto, M. Sato, Y. Yasuda, S. Okazaki, W. Nakamura and S. Mitsui, *J. Soc. Inf. Display*, 2013, **21**, 422.
- F. C. Krebs, J. Fyenbo and M. Jorgensen, *J. Mater. Chem.*, 2010, **20**, 8994-9001.
- K. H. Tsai, J. S. Huang, M. Y. Liu, C. H. Chao, C. Y. Lee, S. C. Hung and C. F. Lin, *J. Electrochem. Soc.*, 2009, **156**, B1188.
- A. K. Pandey and J.-M. Nunzi, *Appl. Phys. Lett.*, 2006, **89**, 213506.
- G. Garcia-Belmonte, A. Munar, E. M. Barea, J. Bisquert, I. Ugarte and R. Pacios, *Org. Electron.*, 2008, **9**, 847.
- N. Tessler, Y. Preezant, N. Rappaport and Y. Roichman, *Adv. Mater.*, 2009, **21**, 2741.
- F. Yang and S. R. Forrest, *ACS Nano*, 2008, **2**, 1022.
- M. J. Frisch, G. W. Trucks, H. B. Schlegel, G. E. Scuseria, M. A. Robb, J. R. Cheeseman, G. Scalmani, V. Barone, B. Mennucci, G. A. Petersson, H. Nakatsuji, M. Caricato, X. Li, H. P. Hratchian, A. F. Izmaylov, J. Bloino, G. Zheng, J. L. Sonnenberg, M. Hada, M. Ehara, K. Toyota, R. Fukuda, J. Hasegawa, M. Ishida, T. Nakajima, Y. Honda, O. Kitao, H. Nakai, T. Vreven, J. A. Montgomery, Jr., J. E. Peralta, F. Ogliaro, M. Bearpark, J. J. Heyd, E. Brothers, K. N. Kudin, V. N. Staroverov, T. Keith, R. Kobayashi, J. Normand, K. Raghavachari, A. Rendell, J. C. Burant, S. S. Iyengar, J. Tomasi, M. Cossi, N. Rega, J. M. Millam, M. Klene, J. E. Knox, J. B. Cross, V. Bakken, C. Adamo, J. Jaramillo, R. Gomperts, R. E. Stratmann, O. Yazyev, A. J. Austin, R. Cammi, C. Pomelli, J. W. Ochterski, R. L. Martin, K. Morokuma, V. G. Zakrzewski, G. A. Voth, P. Salvador, J. J. Dannenberg, S. Dapprich, A. D. Daniels, O.

- Farkas, J. B. Foresman, J. V. Ortiz, J. Cioslowski, and D. J. Fox, Gaussian 09, Revision D.01, Gaussian, Inc., Wallingford CT, 2013.
19. C. J. Brabec, A. Cravino, D. Meissner, N. S. Sariciftci, T. Fromherz, M. T. Rispens, L. Sanchez and J. C. Hummelen, *Adv. Funct. Mater.*, 2001, **11**, 374.
 20. A. Moliton and J. M. Nunzi, *Polym. Int.*, 2006, **55**, 583.
 21. Y. Berredjem, N. Karst, L. Cattin, A. Lakhdar-Toumi, A. Godoy, G. Soto, F. Diaz, M. A. Del Valle, M. Morsli, A. Drici, A. Boulmokh, A. H. Gheid, A. Khelil and J. C. Bernède, *Dyes Pigments*, 2008, **78**, 148.
 22. K. Schulze, C. Uhrich, R. Schüppel, K. Leo, M. Pfeiffer, E. Brier, E. Reinold and P. Bäuerle, *Adv. Mater.*, 2006, **18**, 2872.
 23. H. L. Cheng, Y. S. Mai, W. Y. Chou, L. R. Chang and X. W. Liang, *Adv. Funct. Mater.*, 2007, **17**, 3639.
 24. V. D. Mihailetschi, P. W. M. Blom, J. C. Hummelen and M. T. Rispens, *J. Appl. Phys.*, 2003, **94**, 6849.
 25. M. C. Scharber, D. Mühlbacher, M. Koppe, P. Denk, C. Waldauf, A. J. Heeger and C. J. Brabec, *Adv. Mater.*, 2006, **18**, 789.
 26. B. Zhang, X. W. Hu, M. Q. Wang, H. P. Xiao, X. Gong, W. Yang and Y. Cao, *New J. Chem.*, 2012, **36**, 2042.
 27. V. D. Mihailetschi, L. J. A. Koster, J. C. Hummelen and P. W. M. Blom, *Phys. Rev. Lett.*, 2004, **93**, 216601
 28. D. M. Huang, S. A. Mauger, S. Friedrich, S. J. George, D. Dumitriu-LaGrange, S. Yoon and A. J. Moule, *Adv. Funct. Mater.*, 2011, **21**, 1657
 29. F. C. Tang, J. Chang, F. C. Wu, H. L. Cheng, S. L. C. Hsu, J. S. Chen and W. Y. Chou, *J. Mater. Chem.*, 2012, **22**, 22409.

Table of Contents

Open-circuit voltage shifted by the bending effect for flexible organic solar cells

Wei-Yang Chou*, Chia-Te Yen, Fu-Chiao Wu, Horng-Long Cheng, Shyh-Jiun Liu, and Fu-Ching Tang

Bending effect induced open-circuit voltage shift in flexible OSCs plays important roles in driving the loading devices on flexible circuits.

